PERGAMON

International Journal of Heat and Mass Transfer 46 (2003) 91–100

International Journal of HEAT and MASS TRANSFER

www.elsevier.com/locate/ijhmt

Laminar fluid flow and mass transfer in a standard field and laboratory emission cell

L.Z. Zhang *, J.L. Niu

Department of Building Services Engineering, The Hong Kong Polytechnic University, Kowloon, Hong Kong, China

Received 4 January 2002; received in revised form 12 June 2002

Abstract

The field and laboratory emission cell (FLEC) is becoming a standard method of characterizing pollutant emissions from building materials. Based on this method, the material and the inner surface of the FLEC cap form a cone-shaped cavity. The airflow is distributed radially inward over the test surface through a slit in a circular-shaped channel at the perimeter of the chamber. After mass transfer, the air is exhausted through an outlet in the center. Usually, emission rate profiles are obtained using such cells. However, the local convective mass transfer coefficients are now needed. In this study, laminar fluid flow and mass transfer in a standard FLEC are investigated. The velocity field and moisture profiles are obtained by solving Navier–Stokes equations numerically. The whole geometry, including the air inlet and outlet, channel, air slit, and emission space, are included in the numerical modeling domain. The mean convective mass transfer coefficients are calculated and compared with the experimental data. In the test, distilled water is used in the FLEC lower chamber to substitute the emission surface. Mass transfer data are obtained by calculating humidity differences between the inlet and outlet of a gas stream flowing through the FLEC. The study concentrates on assessing the variations of velocity and humidity profiles, as well as convective mass transfer coefficients, in the cell.

Keywords: Indoor air quality; Field and laboratory emission cell; Mass transfer; Convection

1. Introduction

Volatile organic compounds (VOCs) constitute an important class of indoor-air contaminants. Evidence from a variety of non-industrial building investigations and systematic studies have found that 60% of indoor VOCs come from building materials and furnishings [1]. Various VOCs have been associated with certain symptoms of sick building syndrome, multiple chemical sensitivity, and other health effects. In addition, excessive exposure to VOCs in the work environment can lower people's productivity and cause material and equipment damage [2].

Increased awareness regarding the potential impact of indoor air pollution on health and comfort has resulted in various technical guides for emissions testing of building materials. The current state-of-the-art involves two types of devices: the emission test chamber and the emission cell. The emission test chamber is defined as an enclosure with operational parameters for the determination of VOCs emitted from building products. Typical chamber volumes cover a range from 20 l to 1 m^3 [3]. In case of the emission cell, the surface of the test specimen itself becomes an integral part of the cell and has a high sensitivity due to the large loading ratio (surface area/volume). Today, the best described and most frequently used tool is the so-called field and laboratory emission cell (FLEC) [4]. The emission cell is portable and user-friendly, thus it has become a standard for emission testing in Europe [5,6].

Many tests have been conducted with FLEC, involving various building materials. Clen and co-workers [7] measured the ozone removal rates of selected building products. Wolkoff and Nielsen [8] obtained the diffusion profiles of trans-2-nonenal with FLEC data from

* Corresponding author. Tel.: +852-276-65853; fax: +852-277-46146.

E-mail address: belzhang@polyu.edu.hk (L.Z. Zhang).

0017-9310/03/$ - see front matter
PII: S0017-9310(02)00238-7

Nomenclature

A	area (m^2)
D_v	vapor diffusivity in air mixture (m^2/s)
k	convective mass transfer coefficient (m/s)
p	pressure (pa)
r	radial coordinate (m)
Re	Reynolds number
Sc	Schmidt number
Sh	Sherwood number
u	radial velocity (m/s)
u_m	mean air velocity at the slit (m/s)
v	velocity in angle direction (m/s)
V	volumetric air flow rate (m^3/s)
w	axial velocity (m/s)
z	axial coordinate (m)

Greek symbols

ϕ	angle (rad)
ρ	density (kg/m^3)
θ	dimensionless humidity ratio
ω	humidity ratio (kg vapor/kg air)
v	kinematic viscosity (m^2/s)
δ	spacing between the emission surface and the cap at air slit (m)

Superscript

*	dimensionless

Subscripts

b	bulk
c	cross-section
i	inlet
L	local
m	mean
s	surface
t	transfer

carpet and hexane from sealing material, to name but a few. In these studies, emission rate profiles are obtained for a given air volumetric flow rate. These results are case-specific and only relevant to the test conditions employed. However, to use these emission test data to model pollutant concentrations in real buildings, and also to scale the effects of various control strategies, these profiles are not enough and a more detailed mass transfer model is required. A complete emission model should include three mechanisms: convective mass transfer on surfaces, diffusion in solids, and sorption–desorption with building materials. As an essential part of this process, it is imperative to know the convective mass transfer coefficients in the cell.

The flow geometry of the FLEC is shown in Fig. 1. It is composed of two parts: cap (Fig. 2a) and lower chamber (Fig. 2b). When testing, the planar specimen of the emission material is placed in the lower chamber and becomes an integral part of the emission cell. The upper surface of the specimen (the emission surface) and the inner surface of the FLEC cap form a cone-shaped cavity. The air is supplied through the air slits in the cap. It is introduced through two diametrically positioned inlets (symmetrically placed) into a circular-shaped channel at the perimeter, from where the air is distributed over the emission surface through the circular air slit. The air flows radially inward, until it exits the FLEC outlet in the center.

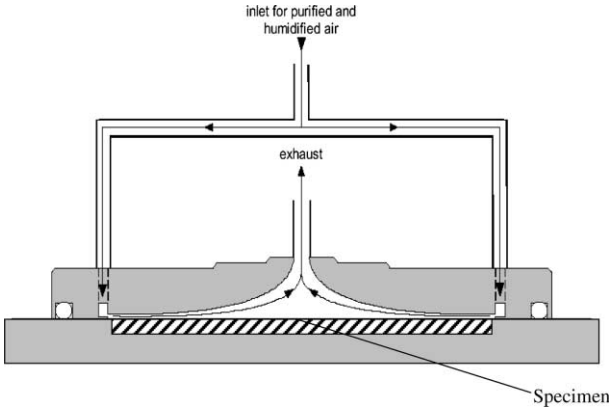

Fig. 1. A schematic showing the flow geometry of the FLEC.

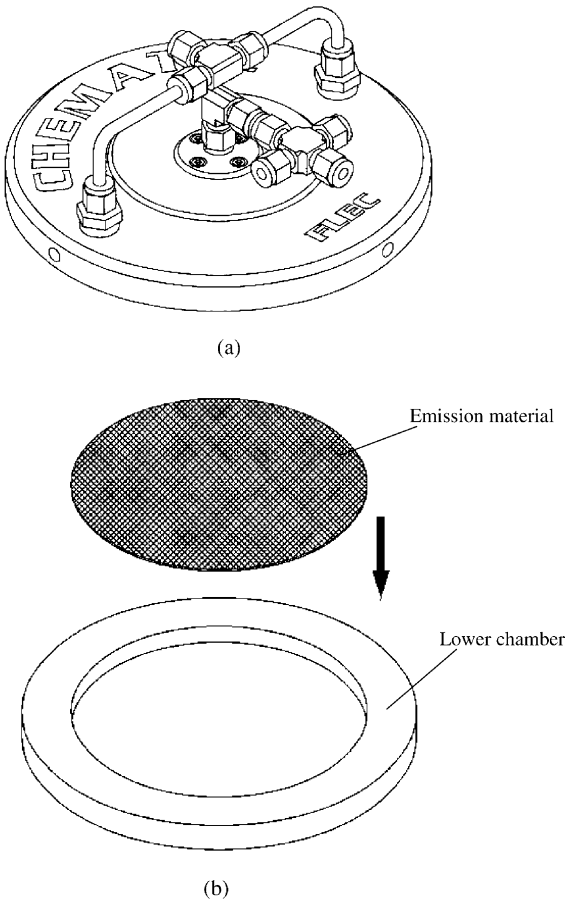

Fig. 2. A view of the FLEC, showing the cap (a) and lower cavity (b).

In addition to emission experiments, forced convection heat mass transfer and fluid flow in cavities of different shapes are of great interest in many other areas. Aggarwal and Talbot [9] used the limiting current electrochemical technique to obtain local mass transfer coefficients in large semi-cylindrical cavities, with the aim of developing a compact artificial lung of high surface area and high mass transfer coefficient. Alkire et al. [10] and Shin and Econmou [11] studied the effect of fluid flow on the rate of mass transfer at the bottom of small rectangular cavities in relation to the etching of masked surfaces, which is used in printed circuit fabrication. Zaki et al. [12] measured the rates of mass transfer at hemispherical cavities machined in the wall of a vertical rectangular duct. Several other workers investigated the heat mass transfer coefficients of radial flow between two parallel disks [13,14] and the flow phenomenon of impinging jets confined by a conical wall [15]. All this research is very interesting. However, studies of mass transfer in a flow geometry like FLEC are still unavailable from open literature. In this study, both numerical simulations and tests will be performed to address this problem.

2. Mathematical models

2.1. Basic equations

For the present situation, the flow is assumed to be laminar and steady. Considering the fluid properties to be constant, the hydrodynamic and mass transfer problem can be described by Navier–Stokes equations in cylindrical coordinates as

Conservation of mass

$$\frac{1}{r^*}\frac{\partial}{\partial r^*}(r^*u^*)+\frac{\partial v^*}{\partial z^*}+\frac{1}{r^*}\frac{\partial w^*}{\partial \phi}=0 \tag{1}$$

where r, z and ϕ are radial, axial and angle coordinates, respectively; u, v, and w are velocities in r, z and ϕ directions (m/s), respectively; superscript '*' in this and the following equations represents dimensionless form.

Conservation of r-momentum

$$u^*\frac{\partial u^*}{\partial r^*}+v^*\frac{\partial u^*}{\partial z^*}+\frac{w^*}{r^*}\frac{\partial u^*}{\partial \phi}=-\frac{\partial p^*}{\partial r^*}+\left[\frac{1}{r^*}\frac{\partial}{\partial r^*}\left(r^*\frac{\partial u^*}{\partial r^*}\right)+\frac{\partial^2 u^*}{\partial z^{*2}}+\frac{\partial^2 u^*}{r^{*2}\partial \phi^2}-\frac{u^*}{r^{*2}}\right] \tag{2}$$

where p represents pressure (pa).

Conservation of z-momentum

$$u^*\frac{\partial v^*}{\partial r^*}+v^*\frac{\partial v^*}{\partial z^*}+\frac{w^*}{r^*}\frac{\partial v^*}{\partial \phi}=-\frac{\partial p^*}{\partial z^*}+\left[\frac{1}{r^*}\frac{\partial}{\partial r^*}\left(r^*\frac{\partial v^*}{\partial r^*}\right)+\frac{\partial^2 v^*}{\partial z^{*2}}+\frac{\partial^2 v^*}{r^{*2}\partial \phi^2}\right] \tag{3}$$

Conservation of ϕ-momentum

$$u^*\frac{\partial w^*}{\partial r^*}+v^*\frac{\partial w^*}{\partial z^*}+\frac{w^*}{r^*}\frac{\partial w^*}{\partial \phi}=-\frac{1}{r^*}\frac{\partial p^*}{\partial \phi}+\left[\frac{1}{r^*}\frac{\partial}{\partial r^*}\left(r^*\frac{\partial w^*}{\partial r^*}\right)+\frac{\partial^2 w^*}{\partial z^{*2}}+\frac{\partial^2 w^*}{r^{*2}\partial \phi^2}\right] \tag{4}$$

Conservation of water vapor

$$u^*\frac{\partial \theta}{\partial r^*}+v^*\frac{\partial \theta}{\partial z^*}+\frac{w^*}{r^*}\frac{\partial \theta}{\partial \phi}=\frac{1}{Sc}\left[\frac{1}{r^*}\frac{\partial}{\partial r^*}\left(r^*\frac{\partial \theta}{\partial r^*}\right)+\frac{\partial^2 \theta}{\partial z^{*2}}+\frac{1}{r^{*2}}\frac{\partial^2 \theta}{\partial \phi^2}\right] \tag{5}$$

where θ is the dimensionless humidity ratio. The characteristic distance is selected as two times the spacing between the emission surface and the cap at the FLEC

perimeter. The mean velocity at the air slit is selected as the characteristic velocity. The dimensionless forms for the variables are expressed as

$$r^* = \frac{r}{2\delta} \tag{6}$$

$$z^* = \frac{z}{2\delta} \tag{7}$$

$$u^* = \frac{2u\delta}{v} \tag{8}$$

$$v^* = \frac{2v\delta}{v} \tag{9}$$

$$w^* = \frac{2w\delta}{v} \tag{10}$$

where δ is the height of space between the emission surface and the FLEC cap at air slit (m); v is the kinematic viscosity (m^2/s).

The dimensionless pressure is defined as

$$p^* = \frac{4p\delta^2}{\rho v^2} \tag{11}$$

where ρ is density (kg/m^3). The dimensionless humidity ratio is given as

$$\theta = \frac{\omega - \omega_s}{\omega_i - \omega_s} \tag{12}$$

where ω is the air humidity ratio (kg vapor/kg air); ω_i represents humidity at the air slit, and ω_s represents humidity at the emission surface.

The Schmidt number is

$$Sc = \frac{v}{D_v} \tag{13}$$

where D_v is vapor diffusivity in the air mixture (m^2/s).

The Reynolds number used to characterize the airflow rate is given by

$$Re = \frac{2u_m\delta}{v} \tag{14}$$

where u_m is the mean air velocity at the slit, and it is calculated by

$$u_m = \frac{V}{2\pi r_0 \delta} \tag{15}$$

where V is the volumetric air flow rate to the FLEC (m^3/s); r_0 is the maximum radius of the emission surface, where air is distributed from the slit (m). The Reynolds numbers for the flow in the FLEC chamber are very small, say, $Re = 21$ when $V = 5$ l/min. Since $Re \ll 2300$, the flow is thought to be laminar.

The Sherwood number is

$$Sh = \frac{2k\delta}{D_v} \tag{16}$$

where k is the convective mass transfer coefficient (m/s).

Now, considering a control volume in the radial direction, the mass balance has

$$kA_t(\omega_s - \omega_b) = -u_m A_c \, d\omega_b \tag{17}$$

where ω_b is the bulk humidity ratio on a cross-section at radius r.

For reasons of symmetry, only half of the FLEC geometry is taken into account, the mass transfer area is

$$A_t = \pi r \, dr \tag{18}$$

The cross-sectional area is

$$A_c = \pi r_0 \delta \tag{19}$$

Substituting Eqs. (18) and (19) into (17), the local mass transfer coefficient is

$$k = -\frac{u_m r_0 \delta}{r(\omega_s - \omega_b)} \frac{d\omega_b}{dr} \tag{20}$$

The local Sherwood number is

$$Sh_L = \frac{r_0^* Re \, Sc}{2\theta_b r^*} \frac{d\theta_b}{dr^*} \tag{21}$$

by considering

$$u_m^* = Re \tag{22}$$

Similarly, the mean Sherwood number is

$$Sh_m = -\frac{r_0^* Re \, Sc}{r_0^{*2} - r^{*2}} \ln \theta_b \tag{23}$$

where the bulk dimensionless humidity ratio is

$$\theta_b = \frac{\int (u^* \theta) \, dA}{u_m^*} \tag{24}$$

The inlet and boundary conditions for mass transfer are

$$r^* = r_0^* : \theta = 1 \tag{25}$$

$$z^* = 0 : \theta = 0 \tag{26}$$

where Eq. (26) indicates that the boundary condition on the emission surface is a uniform concentration condition. Other boundaries are adiabatic surfaces, have no mass transfer, and are expressed as

$$\frac{\partial \theta}{\partial n} = 0 \tag{27}$$

where n is the normal direction.

2.2. Discretisation and solution strategy

For reasons of symmetry, only half of the FLEC is selected as the modeling domain. The Navier–Stokes

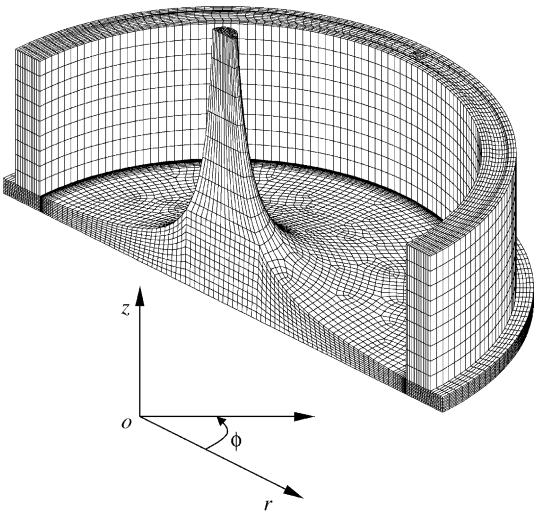

Fig. 3. Discretized meshes of the calculating domain, half of the FLEC, amplified vertically.

equations are solved in three-dimensional cylindrical coordinates. The round channel, which has a rectangular cross-section, the air slit, and the air inlet and outlet vents are meshed as a whole simultaneously. Totally, there are 61318 hexahedral cells in the geometry. The meshes at the entrance region of the flow on the emission surface are finer than those in other locations, to reflect the drastic variations of variables in the boundary layer. The discretised meshes are shown in Fig. 3. The graph is amplified vertically to view the meshes above the emission surface clearly. The computations are performed using the finite volume technique. The derivatives of the diffusive terms in the N–S equations are approximated by second-order central difference and the derivatives of the convective terms by first-order upwind difference. The discretised equations are solved by an iterative procedure and in each step they are solved by the alternating direction implicit (ADI) method. The coupling between velocity and pressure is performed through the SIMPLE algorithm [16]. A relaxation factor of 0.65 is always required in iterations.

The convergence of the iterative procedure is studied following the evolution of the normalized residues. When the normalized residues for mass, velocity and vapor concentration are less than 10^{-5} at every node, the iterations are considered to be converged. The fact is that after 500 iterations, the solution is usually converged, regardless of Reynolds number.

The accuracy of the numerical method is determined from solutions on successively refined grids. The rms error defined by Fletcher [17], and based on the normalized velocity components, is used for that purpose:

$$\mathrm{rms}(u^*) = \left[\left(\sum_i \sum_j \sum_k \left(u^{*1}_{i,j,k} - u^*_{i,j,k} \right)^2 \right) \Big/ m \right]^{1/2} \tag{28}$$

where $u^{*1}_{i,j,k}$ and $u^*_{i,j,k}$ represent quantities calculated with grids having m^1 and m number of nodes, respectively. With the grids mentioned above, the solutions at $V = 509$ ml/min have an rms error lower than 0.011. This value increases with flow rate and is about 0.018 at 1000 ml/min.

3. Experimental studies

The FLEC cell is circular and made of stainless steel, with a diameter of 150 mm and a maximum height of 18 mm. The deepness of the lower chamber is 10 mm. A more detailed description of the structure and parameters of the cell can be found in [5]. When testing, the material is placed on the bottom surface of the lower cavity and becomes an integral part of the emission cell. In this test, to ease the measurement of convective mass transfer coefficients, distilled water is used as the loading material, instead of VOCs emission material. Rather than directly measuring the emission rate profiles of VOCs from building materials, convective surface mass transfer coefficients are calculated by measuring the humidity differences between the inlet and outlet of an air stream, which flows through the FLEC and exchanges moisture with water on the lower surface.

To investigate the local mass transfer coefficients at different FLEC radial locations, seven glass discs with thicknesses of 10 mm and diameters ranging from 130 to 148 mm are prepared. In each test, a disc is placed in the lower chamber and on its bottom surface. Distilled water is injected in the space between the chamber wall and the disc. When finished, the lower chamber, the water, and the glass disk are on the same horizon. Special care is given to ensure the water does not wet the disc's upper surface. With this method, the mass transfer area between the water surface in the FLEC and the air is controlled. A picture showing the placement of a glass disk in the FLEC lower chamber is shown in Fig. 4. When the air flows through the FLEC, it exchanges moisture with the water and is humidified. Since the RH of water on the water surface is 100%, by calculating the humidity differences, the mean convective mass transfer coefficients across the water surface can be calculated. Different discs therefore provide the mean mass transfer coefficients at various FLEC radial locations. To investigate the influences of different gases, both air and N_2 are used in the experiment.

The cell is supplied with clean and humidified air from an air supply unit. The complete test rig is shown in Fig. 5. The supply air flows from a compressed air

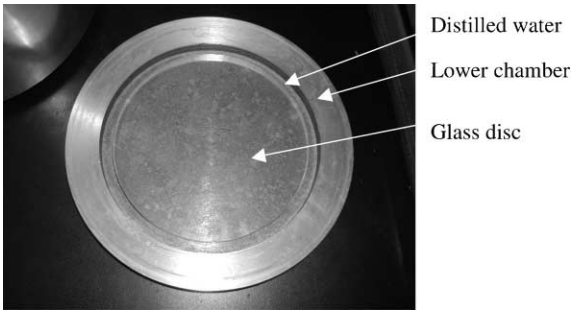

Fig. 4. A picture of the placement of glass disk in the chamber.

bottle and is divided into two streams. One of them is humidified through a bubbler immersed in a bottle of water, and then re-mixed with the other dry air stream. The humidity of the mixed air stream is controlled by adjusting the proportions of air mixing. The airflow rates are controlled by two air pumps/controllers at the inlet and outlet of the FLEC. To prevent outside air from infiltrating into the FLEC, a manometer is installed to monitor the pressure inside the FLEC and ensure that it is positive. The humidities and temperatures inside and outside the FLEC are measured by the built-in RH and temperature sensors, which are installed in the pumps/controllers. The measuring accuracies are respectively 2% for relative humidity, 0.2 °C for temperature, and 2.5% for airflow rate.

Once the humidity differences are measured, the mean mass transfer coefficient is calculated by

$$Sh_{\mathrm{m}} = \frac{V\Delta\omega}{A_{\mathrm{t}}\Delta\varpi} \tag{29}$$

where $\Delta\omega$ is the humidity ratio differences between the air inlet and outlet (kg/kg), A_{t} is the transfer area between the air and water surface (m^2), $\Delta\varpi$ is the logarithmic difference of the humidity ratio between the water surface and the air in FLEC (kg/kg), and Sh_{m} is the mean Sherwood number.

4. Results and discussion

4.1. Local and mean Sherwood numbers

The variations in the measured outlet relative humidity from FLEC with disks of four diameters are plotted in Fig. 6. The inlet humidity is set to a prefixed value and the gas is air. As can be seen, the outlet humidity decreases as the flow rate increases. However, when the diameters are less than 135 mm, the outlet humidity changes little.

The calculated local and mean Sherwood numbers at different FLEC radius under various volumetric flow rates for air are shown in Figs. 7 and 8, respectively. The curves for nitrogen are similar to those for air. These two figures reveal the fact that the Sherwood numbers decrease as the flow progresses. They are very large in the entrance region, and they decrease as the radius decreases, asymptotically approaching the fully developed values. The higher the flow rates (Reynolds numbers), the larger the *Sh* numbers. For flow rates ranging from 186 to 509 ml/min, the mean Sherwood numbers of the whole FLEC emission surface change from 0.05 to 0.2.

The mean Sherwood numbers are also obtained from the experiments. Comparisons of the mean Sherwood numbers between those calculated and experimentally obtained are plotted in Fig. 9. It is shown that the experimentally obtained values are in good agreement with the numerical data. The largest deviation (24%) happens when the *Sh* is very large, namely, at the position near the air slit, where the air begins to flow on the emission surface. This phenomenon may result from the influences of the inlet flow conditions. However, more than 90% of the numerical results are within ±5% deviation from the experimental data.

Fig. 10 represents the variation of the dimensionless bulk humidity against the FLEC radius. The bulk humidity decreases very quickly after the air begins to make contact with the water surface. This means that

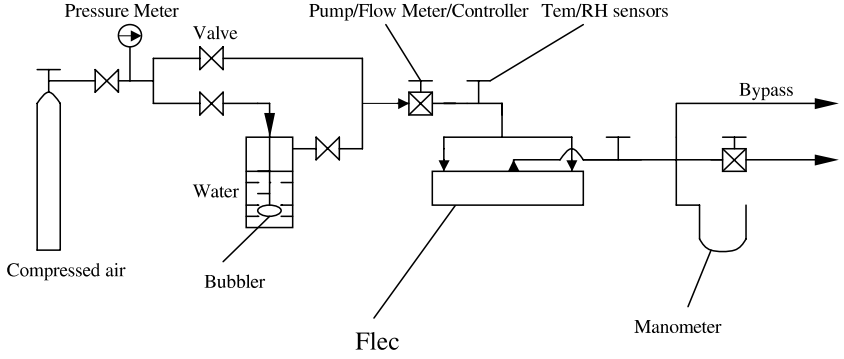

Fig. 5. The set-up of the test apparatus.

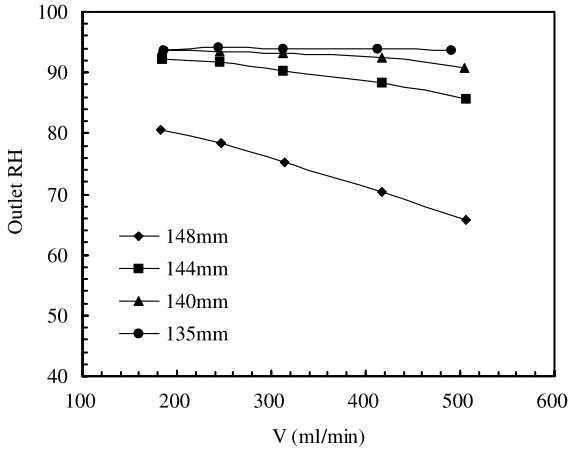

Fig. 6. The outlet relative humidity of air from FLEC with four disks and various flow rates.

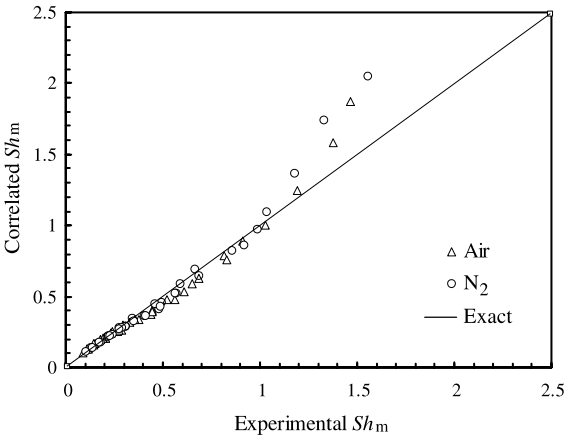

Fig. 9. Comparisons of *Sh* numbers correlated and experimentally obtained.

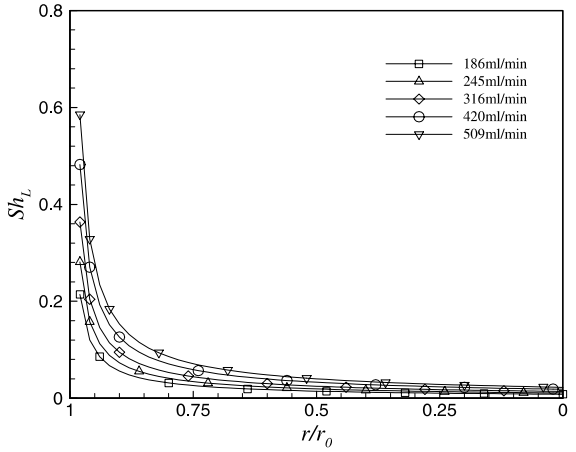

Fig. 7. Local Sherwood numbers along the FLEC radius for air.

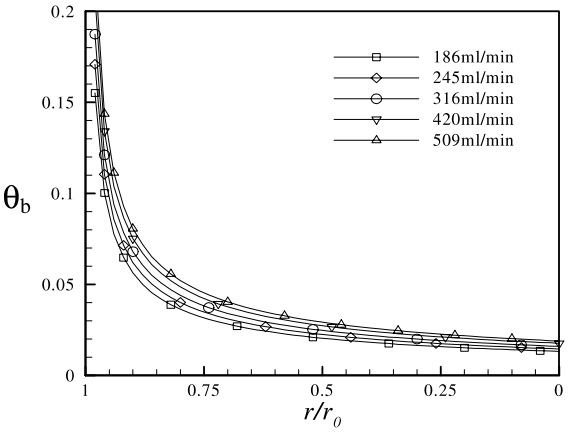

Fig. 10. Dimensionless bulk humidity ratios along the FLEC radius for air.

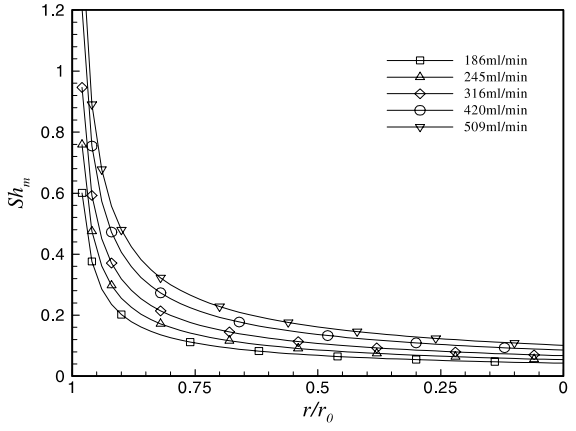

Fig. 8. Mean Sherwood numbers at various FLEC radii for air.

the convective mass transfer coefficients are very large in the first quarter of the FLEC radius along the flow. Under current airflow rate conditions (<509 ml/min), the air becomes nearly saturated in the remaining three quarters of FLEC radius along the flow. This is due to the very small spacing between the emission surface and the FLEC cap (minimum 1 mm). When the air flow rate is increased, the exhaust air becomes less saturated.

For ease of calculation, a multi-variable linear regression technique is used to analyze the local and mean *Sh* numbers, and the bulk humidity. Three correlations have been obtained, as follows:

$$Sh_{\mathrm{m}} = 0.8171 Re^{0.8578} Sc^{0.6790} \left(\frac{r_0 - r}{2\delta}\right)^{-0.6761} \tag{30}$$

$$Sh_{\mathrm{L}} = 0.3359 ReSc \left(\frac{r_0 - r}{2\delta}\right)^{-0.834} \tag{31}$$

$$\theta_b = 0.2076 Re^{0.358} Sc^{0.806} \left(\frac{r_0 - r}{2\delta}\right)^{-0.630} \quad (32)$$

where the validity is for gas with flow conditions of $0 < Re \leqslant 20$.

The maximum deviations between these correlations and the experimental and/or numerical values are 6.8%, 6.4% and 7.6% for mean *Sh*, local *Sh* and θ_b, respectively.

4.2. Flow patterns

Fig. 11 gives an overview of the flow velocity vectors in the cell. The streamlines in a cross-section at $\phi = 90°$ are shown in Fig. 12. The flow inside the FLEC cell can be analyzed in three distinct regions: the impingement region (A), where the flow extends from the inlet to the bottom surface and changes from axial to radial due to the presence of the bottom surface; the radial flow region (B), where the air flows inwardly on the emission surface and exchanges moisture with it; and the exhaust region (C), where the air changes direction from radial to axial and is exhausted at the center of the cell.

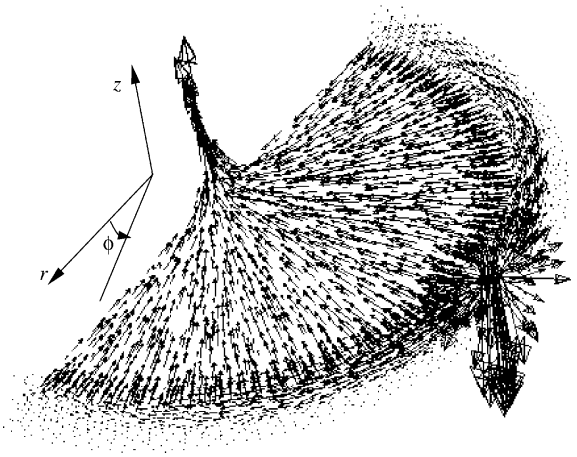

Fig. 11. Three-dimensional velocity vectors in the cell for $V = 509$ ml/min.

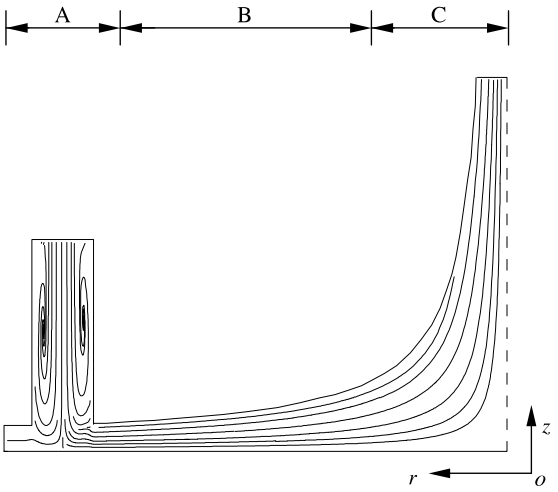

Fig. 12. Streamlines representation in a cross-section ($\phi = 90°$) for $V = 509$ ml/min.

4.2.1. Impingement region

The bottom surface imposes a shift in the air flow direction. The fluid decelerates in the axial direction, losing kinetic energy that is converted into pressure energy. The deceleration starts at the inlet exit and intensifies on approaching the lower surface. The increased pressure is then primarily transformed into the radial momentum of the fluid, while some of it is transformed into flows to other directions. Due to the confinement of the cell walls and the small spacing between the cap and the lower surface, two vortices on both sides of the axis of the air inlet are generated. In other words, in the impingement region and in the vicinity of the inlet, the fluid is occupied by axisymmetric recirculating regions. The rotation axes of the rolls are perpendicular to the inlet flow direction. The recirculating zones diminish with increased angles from the air inlet. Reflecting this fact are the velocity vectors in the symmetry cross-section ($\phi = 90°/180°$), as shown in Fig. 13. In this symmetry plane, the distance to the inlet is so long that no rolls are generated. As a consequence, no vortices can be observed in this figure.

4.2.2. Radial flow region

The flow is distributed radially in the space between the bottom surface and the cap. The FLEC is designed so that the radial-flow cross-section area is invariant with radial location in this region. Therefore, the bulk velocity changes little along the radius. However, the local velocity at the same altitude changes due to different duct heights. The streamlines and the local ve-

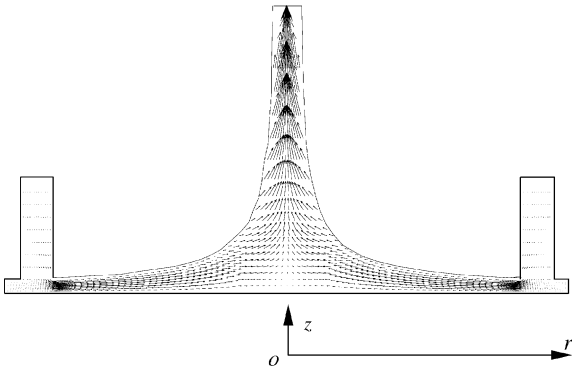

Fig. 13. Velocity vectors in the symmetry cross-section ($\phi = 0°/180°$) for $V = 509$ ml/min, amplified in the z direction.

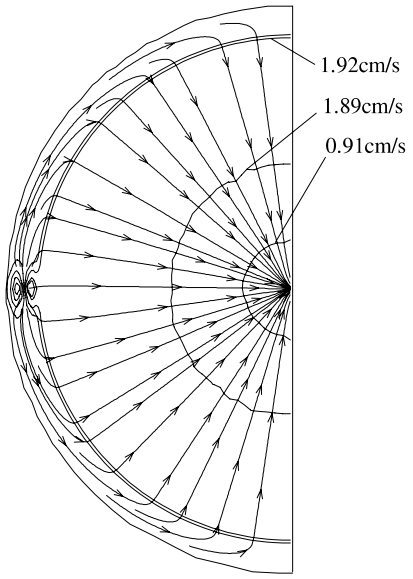

Fig. 14. Streamlines and constant radial velocity profiles in a horizontal cross-section at half the spacing. Lines with arrows are streamlines.

locity contours in a horizontal cross-section at half the spacing are plotted in Fig. 14. When the air low rate is below 1000 ml/min, the mean radial velocity above the emission surface is relatively uniform. It does not vary much with regard to angle and radial locations. However, when the air flow rate is further increased, the flow near the air inlet (in the area of $\phi = 60$–$120°$) becomes demonstrably higher than at other positions. This is obviously the influence of the air inlet.

4.2.3. Exhaust region

The air flows from radial to axial locations and is exhausted in the center. In this region, the radial air velocity is very small, and the resulting mass transfer between the air and the emission surface is negligible.

4.3. Humidity profiles

Due to the small spacing between the cap and the bottom surface, the air will become saturated as it flows along the FLEC radius if the air flow rates are below 1000 ml/min. To see the humidity profiles more clearly, the humidity contours for a larger air flow rate, namely, 2500 ml/min, are discussed. The calculated humidity distribution in a horizontal plate at half the spacing is plotted in Fig. 15. The humidity contours in a vertical cross-section at $\phi = 90°$ are plotted in Fig. 16. The lines in the figures are constant humidity ratio lines. For this case, the inlet temperature and humidity conditions are 23.4 °C and 0.0035 kg/kg, respectively. This figure shows that steep humidity gradients exist in the entry region on

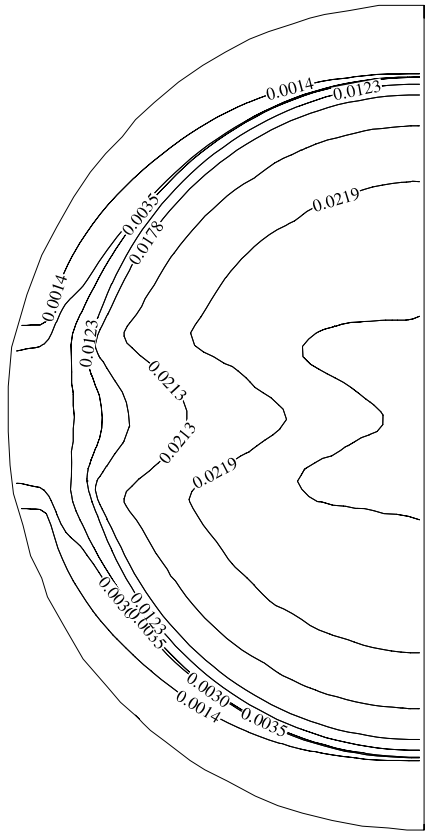

Fig. 15. Humidity profiles in a horizontal cross-section at $z = 0.5$ mm for $V = 5$ l/min.

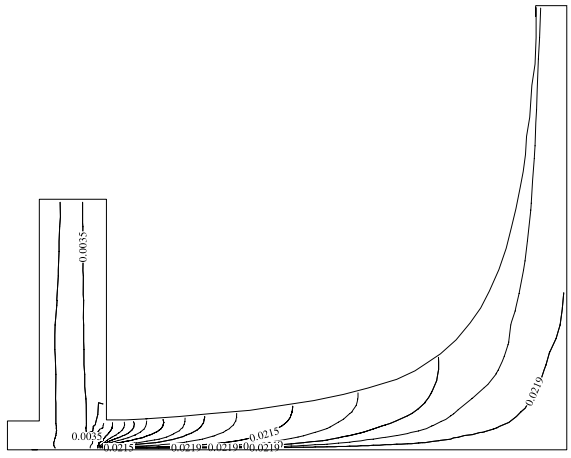

Fig. 16. Humidity profiles in a cross-section ($\phi = 90°$) for $V = 5$ l/min.

the emission surface. When the radius decreases, humidity gradients decrease drastically. This proves that the convective mass transfer coefficient has the largest

value at the beginning of the flow and decreases with the flow's progress. Vertically, humidity gradients are very steep near the emission surface. In addition, under such a flow rate, the air inlet will seriously influence the uniformities of the velocity and humidity fields. As can be seen, unlike the contours under small flow rates, the contours here are not shaped in concentric circles, but in irregular curves.

5. Conclusions

In this study, the fluid flow and convective mass transfer coefficients are experimentally and numerically investigated. Three correlations are summarized to calculate the mean *Sh*, local *Sh* and dimensionless bulk humidity along the chamber radius. For air flow rates below 1000 ml/min, the influences of the inlet on velocity distribution on the emission surface is negligible. The velocity and humidity distributions are uniform and the local mass transfer coefficients are only functions of radial locations. For larger air flow rates, the influences of the inlet on the velocity and humidity fields becomes substantial. Overall, the local mass transfer coefficients are very large in the entrance region, and they decrease as the radius decreases, asymptotically approaching zero at the center of the FLEC. The flow inside the FLEC cell can be analyzed in three distinct regions: the impingement region, the radial flow region, and the exhaust region. The flow in the impingement region is rather complex: around the axis of the inlet, the flow is occupied by axisymmetric recirculating regions. The rotation axes of the rolls are perpendicular to the axis of the inlet. The flow in the other two regions is relatively simple. Under current design airflow conditions, the air becomes nearly saturated shortly after it begins to flow on the emission surface, due to the small spacing between the cap and the bottom surface.

Acknowledgements

This research is funded by the Postdoctoral Fellowship of the Hong Kong Polytechnic University and the PolyU 2000/01 large equipment funding.

References

[1] L. De bellie, F. Haghighat, Y. Zhang, Review of the effect of environmental parameters on material emissions, Proceedings of the Second International Conference on Indoor Air Quality, Ventilation, and Energy Conservation in Buildings, Montreal, Canada, 1995, pp. 111–119.

[2] X. Yang, Q. Chen, A coupled airflow and source/sink model for simulating indoor VOC exposures, Indoor Air 11 (2001) 257–269.

[3] E.C. Spiker, R.P. Hosker, V.J. Corner, J.R. White, R.W. Were, F.L. Harmon, G.D. Gandy, S.I. Sherwood, Environmental chamber for study of the deposition flux of gaseous pollutants to material surfaces, Atmos. Environ. 26A (1992) 2885–2892.

[4] P. Wolkoff, An emission cell for measurement of volatile organic compounds emitted from building materials for indoor use—the field and laboratory emission cell FLEC, Gefahrst.-Reinhalt. L. 56 (1996) 151–157.

[5] CEC-Commission of the European Communities, prENV 13419-2, Building products—determination of the emission of volatile organic compounds—Part 2: emission test cell method, European Committee for Standardization, Brussels, 1998.

[6] E. Uhde, A. Borgschulte, T. Salthammer, Characterization of the field and laboratory emission cell—FLEC: flow field and air velocities, Atmos. Environ. 32 (1998) 773–781.

[7] J.G. Clen, P.A. Clausen, C.J. Weschler, P. Wolkoff, Determination of ozone removal rates by selected building products using the FLEC emission cell, Environ. Sci. Technol. 35 (2001) 2548–2553.

[8] P. Wolkoff, P.A. Nielsen, A new approach for indoor climate labeling of building materials—emission testing, modeling, and comfort evaluation, Atmos. Environ. 30 (1996) 2679–2689.

[9] J.K. Aggarwal, L. Talbot, Electrochemical measurement of mass transfer in semicylindrical hollow, Int. J. Heat Mass Transfer 22 (1979) 61–75.

[10] R.C. Alkire, H. Deligianni, J.B. Ju, Effect of fluid flow on convection transport in small cavities, J. Electrochem. Soc. 137 (1990) 818–824.

[11] C.B. Shin, D.J. Economou, Forced and natural convection effects on the shape evolution of cavities during wet chemical etching, J. Electrochem. Soc. 138 (1991) 527–538.

[12] M.M. Zaki, I. Nirdosh, G.H. Sedahmed, Forced convection mass transfer inside large hemispherical cavities under laminar flow conditions, Chem. Eng. Commun. 159 (1997) 161–171.

[13] C.R. Giovanni, B. Cristiana, S. Aldo, C.S. Giulio, Heat and mass transfer boundary layers in radial creeping flow, Int. J. Heat Mass Transfer 37 (1994) 2145–2153.

[14] A.T. Prata, C.D.M. Pilichi, R.T.S. Ferreira, Local heat transfer in axially feeding radial flow between parallel disks, ASME J. Heat Transfer 117 (1995) 47–53.

[15] J.M. Miranda, J.B.L.M. Campos, Impinging jets confined by a conical wall: laminar flow predictions, AICHE J. 45 (1999) 2273–2285.

[16] S.V. Patankar, Numerical Heat Transfer and Fluid Flow, Hemisphere, Washington DC, 1980.

[17] C.A.J. Fletcher, Computational Techniques for Fluid Dynamics I, Springer Series in Computational Physics, Springer-Verlag, Berlin, 1988.